DOI: 10.1002/cctc.201100503

Methanol-to-Olefin Conversion Catalyzed by Low-Silica AlPO-34 with Traces of Brønsted Acid Sites: Combined Catalytic and Spectroscopic Investigations

Weili Dai,[a, b] Xin Wang,[a] Guanjun Wu,[a] Landong Li,*[a] Naijia Guan,[a] and Michael Hunger*[b]

The reasons for the high activity and long catalyst lifetime of AlPO-34 with a very low molar silicon content [$n_{Si}/(n_{Al}+n_P+n_{Si})=0.01$] in the methanol-to-olefin (MTO) conversion were studied by using in situ FTIR spectroscopy, in situ UV/Vis spectroscopy, and solid-state NMR spectroscopy. The MTO activity of the low-silica AlPO-34 is explained by traces of accessible Brønsted acid sites existing in an isolated manner and characterized by a turnover frequency of 7.0 s^{-1} after a time-on-stream (TOS) of 1 h at 673 K. A contribution of Lewis acid sites to the MTO reaction over low-silica AlPO-34 could be excluded. The high selectivity of low-silica AlPO-34 to light olefins owes to a hydrocarbon pool consisting of benzene-type carbenium ions, as well as dienes. The very few Brønsted acid sites on low-silica AlPO-34 produce a much lower total coke content compared with SAPO-34, leading to an extended catalyst lifetime of the former material.

Introduction

Owing to the increasing demand for light olefins and the limited availability of crude oil, alternative routes for the production of light olefins from nonoil sources are highly desired. The catalytic conversion of methanol to olefins (MTO) over microporous solid acids, which has been known since 1977, has attracted significant attention in the past decades and is now available for commercial application.[1–2] The silicoaluminophosphate SAPO-34 with chabazite cages and 8-ring windows is one of the most interesting candidates for an application as a commercial MTO catalyst. As MTO conversion is an extremely complex process, understanding the reaction mechanism is a great challenge. After long-running debates, a hydrocarbon pool mechanism is accepted as a general feature of the MTO reaction on SAPO-34, consisting of polyalkylaromatics occluded in the cages of the inorganic host, to which methanol and dimethyl ether (DME) are added and from which alkenes are split in a closed cycle.[3–8]

The MTO reaction is an acid-catalyzed reaction, that is, Brønsted acid sites play a key role as active sites in this process. On one side, Brønsted acid sites facilitate the formation of aromatics and carbenium ions during an induction period, which act as hydrocarbon pool species in the working catalyst. On the other hand, polycyclic aromatics are also rapidly formed on Brønsted acid sites and cause the deactivation of MTO catalysts.[9–10] Therefore, attention has been paid for controlling the acid sites to obtain highly active catalyst with long lifetime. A number of methods have been introduced to modify the Brønsted acidity of SAPO-34, for instance, by adjusting the silicon content,[11–13] isomorphous substitution of heteroatoms,[14–16] and silanation.[17] It is reported that lower acidity and longer lifetime of MTO catalysts can be obtained for SAPO-34 with lower silicon contents.[11] Correspondingly, questions arise as to how many Brønsted acid sites are sufficient for the methanol conversion and how a very low quantity of Brønsted acid sites influences the MTO reaction.

AlPO-34 is an aluminophosphate with chabazite-related structure (CHA), that is, it has the same framework as SAPO-34. If silicon impurities are introduced during the synthesis process of AlPO-34, Brønsted acid sites can be created. These acid sites are a result of the substitution of phosphorous by silicon atoms in the AlPO-34 framework leading to the formation of negative framework charges, which are then compensated for by hydroxyl protons. The density of Brønsted acid sites in AlPO-34 caused by traces of framework silicon atoms may be one to two orders lower than that of SAPO-34. Thus, AlPO-34 becomes a good example to investigate the effect of traces of Brønsted sites on the MTO reaction. The present work focuses on the MTO conversion over low-silica AlPO-34 with combined catalytic and spectroscopic investigations. For this purpose, the hydrocarbon pool species formed during the MTO reaction on the catalysts were monitored in situ by FTIR and UV/Vis spectroscopy. Furthermore, catalyst samples were taken during the MTO reaction and transferred from the fixed-bed reactor to MAS NMR rotors without contact to air for solid-state ^1H and ^{13}C NMR studies.

[a] Dr. W. Dai, Dr. X. Wang, Dr. G. Wu, Prof. L. Li, Prof. Dr. N. Guan
Key Laboratory of Advanced Energy Materials Chemistry
(Ministry of Education)
Nankai University, College of Chemistry
Tianjin 300071 (P.R. China)
E-mail: lild@nankai.edu.cn

[b] Dr. W. Dai, Prof. Dr. M. Hunger
University of Stuttgart
Institute of Chemical Technology
Fax: (+49) 0711-68564081
E-mail: michael.hunger@itc.uni-stuttgart.de

Results and Discussion

Characterization of the catalyst materials

The powder XRD patterns of the calcined catalysts are shown in Figure 1. Typical diffraction lines are observed for SAPO-34, indicating that this material is a pure phase;[18] the powder XRD pattern of AlPO-34 is in agreement with a previous report.[19] The significant differences in the XRD patterns of AlPO-34 and SAPO-34 are because of a low-temperature triclinic distortion of the CHA framework in AlPO-34. The very weak, broad background in the pattern for SAPO-34 may be a result of amorphous impurities, which must be present at very low levels, considering the good quality of the SEM image and the high BET surface area of this material in comparison with AlPO-34 (see below).

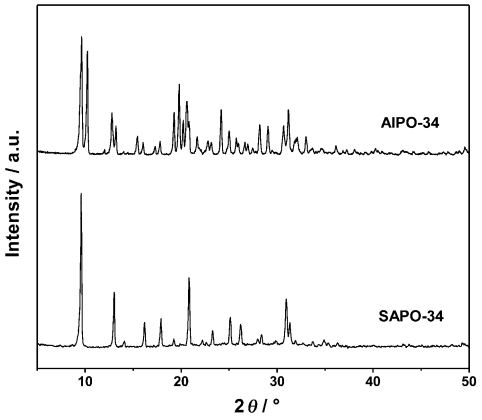

Figure 1. XRD patterns of the calcined SAPO-34 (bottom) and AlPO-34 (top).

The crystal morphologies of the as-synthesized samples are shown in Figure 2. The SAPO-34 and AlPO-34 crystals appear as cuboids and rhombuses, respectively, with crystal sizes of 5–10 μm.

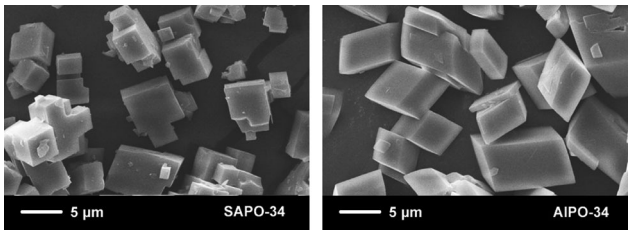

Figure 2. SEM images of the as-synthesized SAPO-34 (left) and AlPO-34 (right).

The chemical compositions and BET surface areas of the calcined samples are given in Table 1. The molar silicon content of SAPO-34 is $n_{Si}/(n_{Al}+n_P+n_{Si}) = 0.17$, whereas that of AlPO-34 is 0.01. This indicates that a very low amount of silicon was introduced into AlPO-34. The surface areas of the calcined SAPO-34 and AlPO-34 are 464 and 332 m^2g^{-1}, respectively, indicating the intactness and accessibility of the pore systems.

Table 1. Chemical compositions and surface areas of the calcined samples under study.

Samples	Elemental analysis[a] [mmol g^{-1}]				BET surface area[b] [$m^2 g^{-1}$]
	n_{Al}	n_P	n_{Si}	$n_{Si}/(n_{Si}+n_{Al}+n_P)$	
SAPO-34	6.19	4.63	2.23	0.17	464
AlPO-34	6.90	6.62	0.14	0.01	332

[a] Determined by inductively coupled plasma atomic emission spectroscopy. [b] Determined by N_2-adsorption.

Catalytic studies

The methanol conversion and product selectivity over SAPO-34 and low-silica AlPO-34 at different reaction temperatures after the initial 5 min are shown in Table 2. For SAPO-34, 83.5% methanol conversion, with DME as the major product, was obtained at 523 K. By increasing the reaction temperature from 523 to 723 K, the methanol conversion increased to 100%, whereas the DME selectivity decreased to zero. For AlPO-34, the same trend as for SAPO-34 was observed. At 523–623 K, the methanol conversion and olefin selectivity were lower for low-silica AlPO-34 than for SAPO-34 at the same reaction temperatures. However, after raising the reaction temperature to 673 K, a methanol conversion of 100% with an olefin selectivity of >90% was obtained both for SAPO-34 and AlPO-34. Hence, comparable amounts of light olefins were formed at high reaction temperatures over both catalysts.

Table 2. Results of the MTO conversion over SAPO-34 and AlPO-34 at different reaction temperatures.

Sample	Reaction temperature [K]	Methanol conversion [%]	Product selectivity [%]		
			$C_2^=$–$C_4^=$[a]	DME	others
SAPO-34	523	83.5	30.3	67.4	2.3
	573	93.4	82.7	10.6	6.7
	623	100	89.8	1.9	8.3
	673	100	91.5	0	8.5
	723	100	91.8	0	8.2
AlPO-34	523	60.5	0.0	100	0.0
	573	83.3	8.1	91.8	0.1
	623	88.9	50.9	45.5	3.6
	673	100	90.1	0	9.9
	723	100	90.7	0	9.3

[a] Ethane, propene, and butenes.

To get detailed information on hydrocarbon pool compounds formed in the catalyst cages during the MTO reaction, the fate of active surface species during the catalyst lifetime, and the catalyst deactivation, we investigated the methanol conversion at 673 K. In Figure 3, the time dependence of the

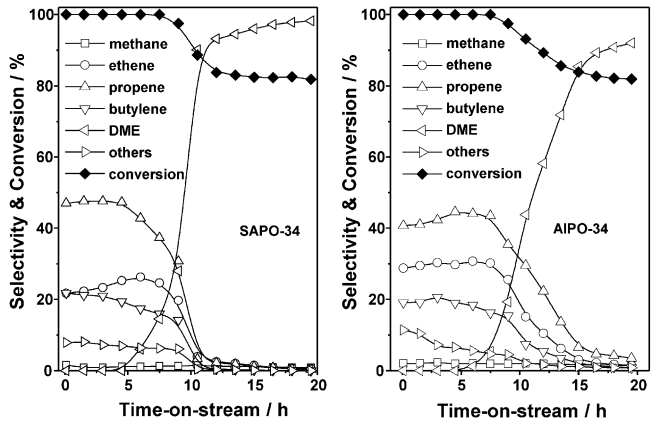

Figure 3. Methanol conversion and product selectivity during the MTO conversion over SAPO-34 and low-silica AlPO-34 at 673 K up to a TOS of 20 h.

methanol conversion and product selectivity over SAPO-34 (left) and low-silica AlPO-34 (right), determined in a fixed-bed reactor at 673 K, are shown. SAPO-34 exhibits a methanol conversion of 100% with a selectivity of $>90\%$ to C_2–C_4 olefins at the time-on-stream (TOS) of 4.5 h. After a TOS of 10.5 h, the selectivity to C_2–C_4 olefins gradually decreases to 10%, whereas the methanol conversion is 85%. For low-silica AlPO-34, a methanol conversion of 100% with a selectivity to C_2–C_4 olefins of $>90\%$ is maintained up to a TOS of 7.5 h. At a TOS of 10.5 h, a selectivity to C_2–C_4 olefins of 55% could be obtained at a methanol conversion of 90%. At a TOS of 20 h, DME is formed exclusively on the SAPO-34, whereas AlPO-34 produces 5% propene. Hence, the deactivation of low-silica AlPO-34 is slower than that of SAPO-34 and it exhibits a better MTO performance compared with SAPO-34 at 673 K.

In situ FTIR, UV/Vis, and solid-state NMR spectroscopy of organic deposits

The nature of organic compounds formed during the MTO conversion over the catalysts under study was investigated by in situ FTIR and UV/Vis spectroscopy at 673 K. Figure 4 shows the FTIR spectra of the organic species formed on SAPO-34 (top) and low-silica AlPO-34 (bottom). For SAPO-34, strong bands at 2873 cm^{-1} and 2925 cm^{-1} caused by the stretching vibrations of C–H bonds and weak bands at 1608 cm^{-1}, 1503 cm^{-1}, 1461 cm^{-1}, and 1380 cm^{-1} caused by C=C vibrations of aromatics and bending vibrations of the C–H bonds[20–23] are observed. The intensities of these bands increased with the progress of the MTO reaction. Additionally, two strong bands occurred at 3017 cm^{-1} and 1304 cm^{-1} corresponding to C-H stretching and methyl bending vibrations of dienes.[24] For SAPO-34, the intensities of these two bands increased at first with increasing TOS, but then decreased gradually.

The FTIR spectra of organic species formed on low-silica AlPO-34 are slightly different to those obtained for SAPO-34 in terms of the band intensities and wavenumbers. The bands in the ranges of 2825–2955 cm^{-1} and 1345–1608 cm^{-1} observed for low-silica AlPO-34 are significantly lower than those of SAPO-34 indicating that much less hydrocarbons are formed. The steady increase of the bands at 3017 cm^{-1} and 1304 cm^{-1} in the case of low-silica AlPO-34 hints to a continuous and increasing formation of dienes.

The UV/Vis spectra recorded during the initial 5 min of the methanol conversion over SAPO-34 at 673 K (Figure 5, top) consist of bands caused by dienes (240 nm), polyalkylaromatics (270 nm), monoenylic carbenium ions (300 nm), and benzene-type carbenium ions (390 nm) indicating a rapid formation of these species.[25–27] With further progress of the MTO reaction, monoenylic carbenium ions are gradually transformed into dienylic carbenium ions (350 nm). For low-silica AlPO-34, the bands of dienes are observed exclusively during the initial 5 min and the bands of polyalkylaromatics and benzene-type carbenium ions appear with the progress of the reaction; this fits well with the results of in situ FTIR spectroscopy. In comparison with SAPO-34, the UV/Vis bands of polyalkylaromatics and benzene-type carbenium ions are much weaker for low-silica AlPO-34.

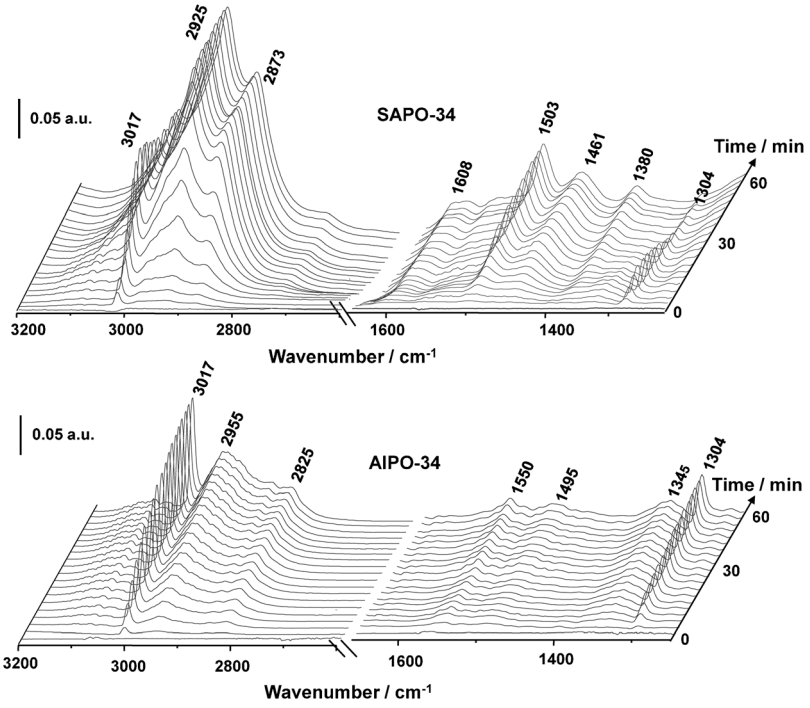

Figure 4. In situ FTIR spectra recorded during MTO conversion over SAPO-34 and low-silica AlPO-34 at 673 K up to a TOS of 1 h.

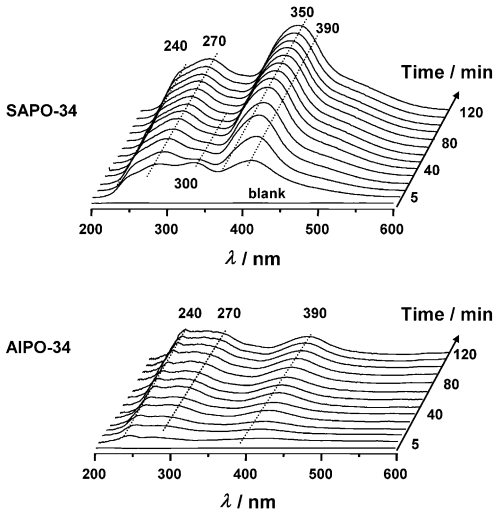

Figure 5. In situ UV/visspectra recorded during MTO conversion over SAPO-34 and low-silica AlPO-34 at 673 K up to a TOS of 2 h.

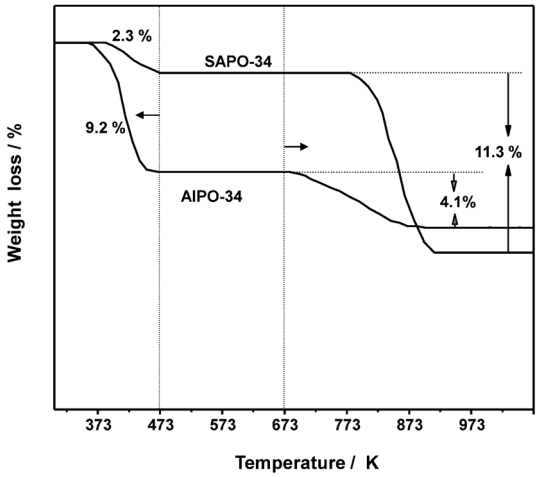

Figure 6. TGA curves of used SAPO-34 and low-silica AlPO-34 catalysts obtained after MTO conversion at 673 K for a TOS of 10.5 h.

The thermogravimetric analysis (TGA) curves in Figure 6 give the total contents of organic deposits on the used SAPO-34 and low-silica AlPO-34 catalysts. These curves were recorded after MTO conversion at 673 K for a TOS of 10.5 h. In general, two clear weight losses can be recognized: a low-temperature weight loss at $<$473 K and a high-temperature weight loss at $>$673 K. These are ascribed to desorption of volatile species and occluded organic deposits, respectively. For the used SAPO-34 catalyst, a weight content of occluded organic deposits of 11.3% was determined, whereas this weight content for the used AlPO-34 catalyst was 4.1%. For AlPO-34, therefore, the probability of pore-blocking as a reason for catalyst deactivation is much lower than for SAPO-34. These results are in good agreement with the results of in situ FTIR and UV/Vis spectroscopy, which both hint at a much lower organic deposit content on the used low-silica AlPO-34 catalyst.

Solid-state NMR studies of surface species

The catalytic studies clearly indicate a good MTO performance and extended catalyst lifetime of low-silica AlPO-34, which has only 6% of framework silicon species in comparison with SAPO-34. In this connection, the question arises as to whether Brønsted acid sites alone or both Brønsted and Lewis acid sites have to be discussed as catalytically active surface sites on low-silica AlPO-34.

^{13}C-2-acetone ($CH_3{}^{13}COCH_3$) is a probe molecule utilized in ^{13}C MAS NMR spectroscopy for distinguishing Brønsted (210–225 ppm) and Lewis acid sites (225–266 ppm).[28–31] Figure 7 presents ^{13}C MAS NMR spectra of the calcined (673 K) SAPO-34 (top) and low-silica AlPO-34 (bottom) recorded after adsorption of ^{13}C-2-acetone. For SAPO-34, a signal of adsorbed ^{13}C-2-acetone is observed at 217 ppm with a low-field shoulder at approximately 224 ppm. The signal at 217 ppm is characteristic of acetone adsorbed at Brønsted acid sites of silicoaluminophosphates,[31] whereas the low-field shoulder at approximately 224 ppm hints at a low number of weak Lewis acid sites.[29,30] For AlPO-34, weak signals of acetone interacting with Brønsted acid sites at 211 and 215 ppm and a narrow signal caused by physisorbed acetone (205 ppm) occurred after adsorption of ^{13}C-2-acetone. However, no ^{13}C MAS NMR signals of acetone molecules interacting with Lewis acid sites at 225-266 ppm could be observed.[29,30] This indicates that a contribution of Lewis acid sites to the MTO reaction over low-silica AlPO-34 can be excluded.

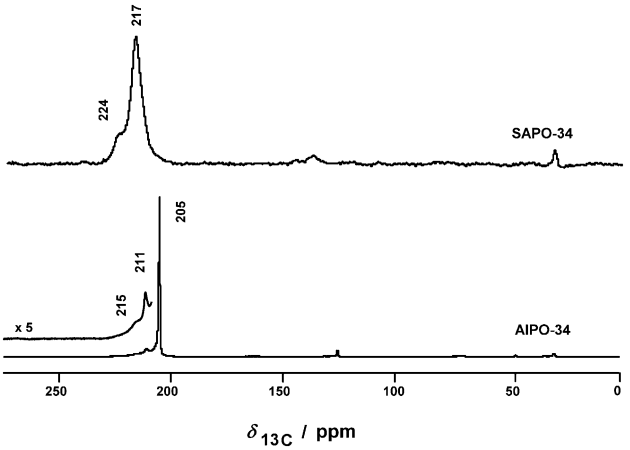

Figure 7. ^{13}C MAS NMR spectra of dehydrated (673 K) samples recorded after loading of ^{13}C-2-acetone on calcined SAPO-34 and low-silica AlPO-34.

Focusing on the properties of Brønsted acid sites, ^{1}H MAS NMR spectroscopy of the calcined and used SAPO-34 and low-silica AlPO-34 catalysts upon different TOS was performed. The spectrum of the calcined SAPO-34 (Figure 8, top, left) is dominated by the signal of Brønsted acidic bridging OH groups (SiOHAl) at 3.7 ppm.[31,32] Loading of ammonia on SAPO-34 and low-silica AlPO-34 results in a protonation of the probe molecules by accessible Brønsted acid sites and the occurrence of an ^{1}H MAS NMR signal of ammonium ions at

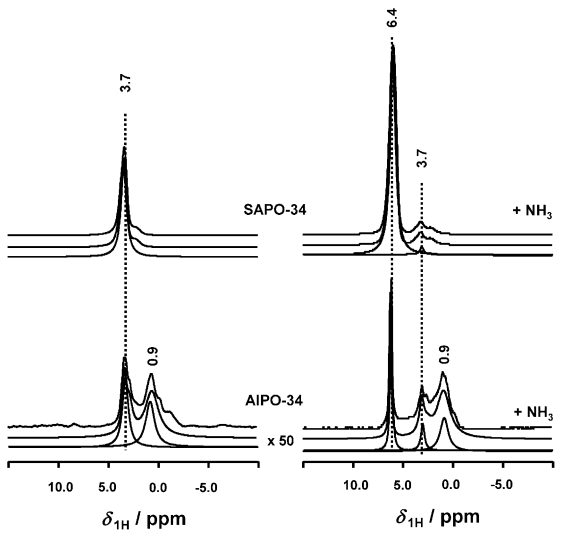

Figure 8. ^{1}H MAS NMR spectra of the calcined SAPO-34 and low-silica AlPO-34 recorded before (left) and after (right) adsorption of ammonia. From top to bottom, the experimental spectra, the simulated spectra, and the signal components utilized for simulation are shown.

6.4 ppm. This signal has an intensity that is a factor of four times as large as the signal of the initial acidic hydroxyl groups. The quantitative evaluation of the ammonium signal of the calcined and ammonia-loaded SAPO-34 (TOS of 0 min) gave a value of 1.0 mmol g^{-1} accessible Brønsted acid sites (Figure 8, top, right, and Table 3, column 4). The weak signal at 3.7 ppm occurring after the ammonia-loading (Figure 8, top, right) owes to nonaccessible SiOHAl groups.

Table 3. Numbers of accessible SiOHAl groups (n_{SiOHAl}) and benzene-based carbenium ions ($n_{benzenium}$) on the calcined and used catalysts, as determined by quantitative ^{1}H MAS NMR spectroscopy for different times on stream determined upon ammonia adsorption.

Catalyst	TOS	n_{SiOHAl}[a] [mmol g^{-1}]	$n_{benzenium}$[a] [mmol g^{-1}]
SAPO-34	0	1.000	0
SAPO-34	5 min	0.433	0.101
SAPO-34	1 h	0.194	0.322
SAPO-34	10 h	≈0	≈0
AlPO-34	0	0.012	0
AlPO-34	5 min	0.004	0.001
AlPO-34	1 h	0.001	0.002
AlPO-34	10 h	≈0	≈0

[a] Experimental accuracy = ±5%.

For the calcined low-silica AlPO-34, the number of Brønsted acid sites reacting with ammonia to form ammonium ions was found to be 0.01 mmol g^{-1} (Figure 8, bottom, right, and Table 3, column 4), that is, only 1% of that observed for calcined SAPO-34. This means that traces of Brønsted acid sites are formed on low-silica AlPO-34 by introducing a very small amount of silicon atoms into the catalyst framework. The signal at approximately 0.9 ppm in the spectrum of AlPO-34 is caused by AlOH groups at framework defects and the crystal surfaces.[31,32] This signal remained almost unchanged after ammonia-loading, which indicates that these hydroxyl groups do not react with ammonia caused by their low acidity.

To investigate the fate of Brønsted acid sites and the active hydrocarbon pool species on the used SAPO-34 and low-silica AlPO-34 catalysts by ^{1}H MAS NMR spectroscopy, samples were taken from the fixed-bed reactor at TOSs of 5 min, 1 h, and 10.5 h, which represent the initial state, the steady-state, and the deactivated state of the MTO catalysts, respectively. The ^{1}H MAS NMR spectrum of low-silica AlPO-34 taken at a TOS of 5 min (Figure 9a, left) consists of signals at 0.8–2.2 ppm and

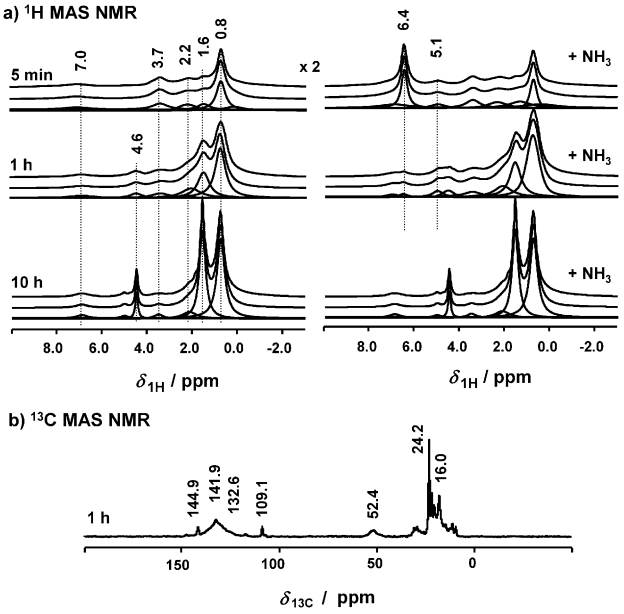

Figure 9. ^{1}H MAS NMR spectra of used AlPO-34 catalysts obtained after different TOS (5 min, 1 h, and 10 h) recorded before (left) and after (right) adsorption of ammonia (a). From top to bottom: the experimental spectra, the simulated spectra, and the signal components utilized for the simulation are shown. In (b), ^{13}C MAS NMR spectrum of used AlPO-34 obtained after a TOS of 1 h.

7.0–8.0 ppm caused by hydrogen atoms in aliphatic and aromatic compounds, respectively. The signals that occur at 5.1 and 6.4 ppm after adsorption of ammonia (Figure 9a, right) are attributed to phenylammonium ions and ammonium ions formed upon protonation of ammonia by benzene-based carbenium ions and accessible SiOHAl groups, respectively. For the low-silica AlPO-34 catalyst taken at a TOS of 1 h and loaded with ammonia, the ^{1}H MAS NMR signal of phenylammonium ions at 5.1 ppm increased, whereas the signal of ammonium ions at 6.4 ppm formed by chemisorption of ammonia on accessible bridging OH groups significantly decreased. Furthermore, a signal caused by dienes appeared at 4.6 ppm with an intensity increasing distinctly up to a TOS of 10 h. In contrast, this signal is not observed for the used SAPO-34 catalysts treated under the same conditions (Figure 10).

To confirm the above-mentioned assignments of the ^{1}H MAS NMR signals of the hydrocarbon pool species,

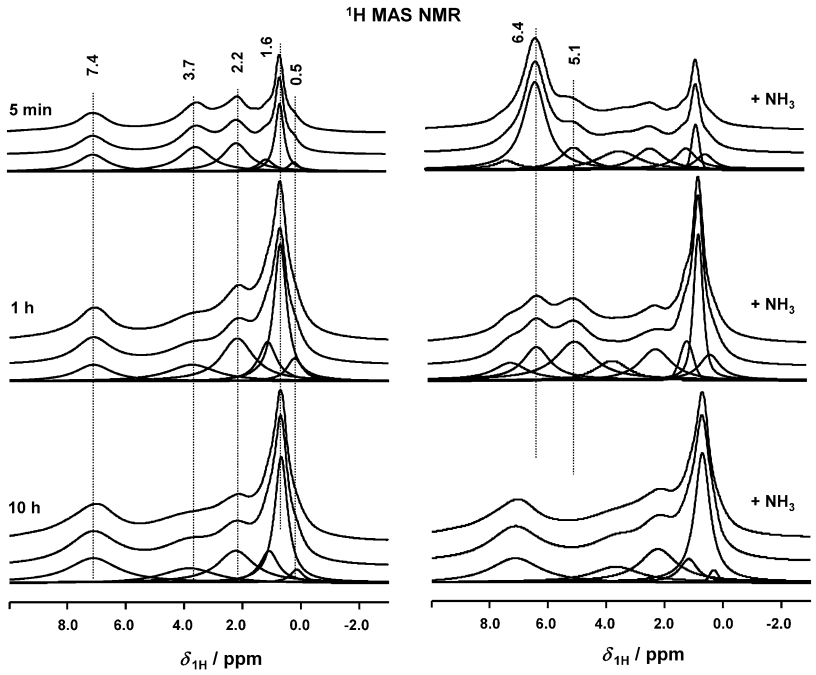

Figure 10. ^{1}H MAS NMR spectra of used SAPO-34 catalysts obtained after different TOSs (5 min, 1 h, and 10 h), recorded before (left) and after (right) adsorption of ammonia. From top to bottom, the experimental spectra, the simulated spectra, and the signal components utilized for the simulation are shown.

^{13}C MAS NMR spectroscopy of a used low-silica AlPO-34, prepared by conversion of ^{13}C-enriched methanol at 673 K for a TOS of 1 h, was performed. The ^{13}C MAS NMR spectrum in Figure 9b consists of signals at 16–25 ppm and 126–135 ppm caused by carbon atoms of alkyl groups and aromatic compounds, respectively.[33] The ^{13}C MAS NMR signal at 52.4 ppm is caused by C_1 carbon atoms of benzene-based carbenium ions,[34–36] whereas the sharp signals at 109.1 and 144.9 ppm support the formation of dienes. The latter signals could be caused by 2,3-dimethyl-1,3-butadiene ($\delta_{13C}=113.0$ and 143.8 ppm; $\delta_{1H}=4.9$ and 1.9 ppm) or 5-methyl-1,4-diethyl-cyclopentadiene ($\delta_{13C}=24.7$, 124.3, and 144.8 ppm; $\delta_{1H}=4.7$, 2.2, and 1.1 ppm).[37]

The intensities of the ^{1}H MAS NMR signals at 7.0–8.0 ppm, which are caused by hydrogen atoms of aromatics and coke deposits, are significantly larger in the spectra of used SAPO-34 in comparison with those of used low-silica AlPO-34 (Figure 9 and 10). This agrees qualitatively with the results of TGA (Figure 6). However, the weight loss determined by TGA depends mainly on the loss of carbon atoms and not on the loss of hydrogen atoms. Furthermore, the C/H ratios are very different for different aromatic and polyaromatic compounds. Therefore, no direct quantitative comparison of TGA and ^{1}H MAS NMR data obtained for aromatic and coke deposits is possible.

Quantitative evaluation of the ^{1}H MAS NMR spectra of SAPO-34 and low-silica AlPO-34 catalysts recorded after loading of ammonia gave the number of accessible Brønsted acid sites and benzene-based carbenium ions as a function of the MTO conversion time (Table 3, columns 4 and 5). Whereas the calcined low-silica AlPO-34 sample has 0.01 mmol g^{-1} accessible Brønsted acid sites, this site density decreased to 0.004 mmol g^{-1} after a TOS of 5 min. At the same time, 0.001 mmol g^{-1} benzene-based carbenium ions (1% of that on SAPO-34) are formed. After a TOS of 1 h, the number of accessible Brønsted acid sites decreased to 0.001 mmol g^{-1}, whereas the number of accessible polyalkylbenzenium ions increased to 0.002 mmol g^{-1}. For the strongly deactivated SAPO-34 and low-silica AlPO-34 catalysts obtained after a TOS of 10.5 h, neither accessible Brønsted acid sites nor benzene-based carbenium ions could be detected. These observations indicate that a very low number of accessible SiOHAl groups (0.01 mmol g^{-1}), that is, 0.03 Brønsted acid sites per cage corresponding to a mean site distance of 42 nm, are responsible for the high catalytic activity of low-silica AlPO-34 in the MTO reaction. In this case, the reactants and initial reaction products have short contact times at the Brønsted acid sites of low-silica AlPO-34, which is enough to form a few benzene-based carbenium ions, causing the MTO conversion according to the hydrocarbon pool mechanism. On the other hand, the much shorter average acid site distance of 0.58 nm in SAPO-34 increases the contact time of reactants at Brønsted acid sites. This leads to the rapid formation of large organic deposits, which cover the Brønsted acid sites, block micropores and cages, and cause the more rapid deactivation of SAPO-34 compared to the low-silica AlPO-34.

Interestingly, a similar effect of an extension of the lifetime of CHA-type MTO catalysts with decreasing Brønsted site density was observed by Sommer et al. for SSZ-13 zeolites.[38] The n_{Si}/n_{Al} ratios of 16 and 131 of the parent SSZ-13 materials studied in their work correspond to Brønsted site densities differing by a factor of approximately 10. They observed a significantly longer catalyst lifetime for the SSZ-13 material with the lower acid site density.[38] Because of the much stronger Brønsted acid sites of aluminosilicate-type SSZ-13 in comparison with silicoaluminophosphate-type SAPO-34 however, the deactivation of the SSZ-13 zeolite with $n_{Si}/n_{Al}=16$ was already completed after a TOS of 30 min, whereas the SSZ-13 zeolite with $n_{Si}/n_{Al}=131$ reached a catalyst lifetime of a TOS of 40 min.

The density of accessible Brønsted acid sites in low-silica AlPO-34 of 0.001 mmol g^{-1} determined after a TOS of 1 h and the parameters of the MTO reaction (conversion of 100% at 673 K) lead to a turnover frequency (TOF) of 7.0 s^{-1}. This TOF value is significantly higher in comparison with the TOF value of 1.2 s^{-1} determined for MTO conversion over SAPO-34 in an earlier study.[39] An important reason for the high TOF value of

Brønsted acid sites in low-silica AlPO-34 could be their isolated character and their much lower blocking by organic deposits. On the other hand, these Brønsted acid sites are not only responsible for the formation of light olefins, but also for the formation of organic deposits. Hence, the higher TOF of acid sites in low-silica AlPO-34 also leads to the higher coke content per acid site compared with SAPO-34.

Conclusions

AlPO-34 with a very low silicon content in the framework [$n_{Si}/(n_{Al}+n_P+n_{Si})=0.01$] was prepared and applied as a methanol-to-olefin conversion (MTO) catalyst at 673 K, with a SAPO-34 [$n_{Si}/(n_{Al}+n_P+n_{Si})=0.17$] material as a reference catalyst. The MTO activity and product selectivity of the low-silica AlPO-34 at 673 K was found to be comparable with those of SAPO-34, but a longer catalyst lifetime occurred for the former material. By quantitative ^{1}H MAS NMR spectroscopy of calcined and used MTO catalysts taken from the fixed-bed reactor after different times on stream (TOSs), the number of accessible Brønsted acid sites was determined. According to these studies, the low-silica AlPO-34 has maximum 1% of accessible Brønsted acid sites in comparison with SAPO-34 under same conditions. These very few acid sites exist in a very isolated manner. The presence of Lewis acid sites on low-silica AlPO-34 could be excluded.

In situ FTIR, UV/Vis, and solid-state NMR spectroscopy of the used MTO catalysts performed after different TOSs indicated that benzene-type carbenium ions and polyalkylaromatics are formed on low-silica AlPO-34 as on SAPO-34, but with a significantly lower content on the former material. Benzene-type carbenium ions are discussed as active hydrocarbon pool compounds and may be responsible for the high selectivity of the above-mentioned catalysts to light olefins. As a significant difference between low-silica AlPO-34 and SAPO-34, a high content of dienes was observed on the working low-silica AlPO-34 catalyst. With increasing TOS, very different hydrocarbon pool coverages were found by in situ FTIR, UV/Vis, and solid-state NMR spectroscopy for low-silica AlPO-34 and SAPO-34, which is in agreement with the different coke contents of the used catalysts, as determined by thermogravimetric analysis.

To summarize, the very low density of Brønsted acid sites on the low-silica AlPO-34 catalyst has a positive effect on the activity and product selectivity of this material in the MTO conversion in comparison to SAPO-34 and increases the catalyst lifetime. One of the reasons for this interesting catalytic property may be the different composition of the hydrocarbon pool, in which there is a higher content of dienes and a much lower formation of large aromatics.

Experimental Section

SAPO-34 and low-silica AlPO-34 were synthesized by hydrothermal methods following the procedures described in the literature,[18,19] in the case of AlPO-34, by using pseudo-boehmite as aluminum source containing traces of silicon. The as-synthesized materials were heated with a rate of 2 K min^{-1} to 973 K in an oven under flowing synthetic air (60 L h^{-1}, 20 vol% oxygen) for 4 h to totally remove the occluded organic structure-directing agents and to exclude effects of organic impurities on the catalytic properties of the materials under study.[40]

X-ray diffraction patterns of the as-synthesized and calcined samples were recorded on a Bruker D8 diffractometer with CuK_α radiation ($\lambda=1.5418$ Å) at 5–50° with a scan speed of $2\theta=6.0°$ min^{-1}. A HITACHI S-4700 scanning electron microscope was used for studying the crystal morphologies of the samples. The SEM images were recorded on samples covered with a thin layer of gold, deposited by sputtering. The chemical compositions of the calcined samples were determined by inductively coupled plasma atomic emission spectroscopy. The surface areas of the catalysts were obtained by means of nitrogen adsorption measurements performed at 77 K on a Quantachrome Autosorb 3B instrument. Before N_2 adsorption, the samples were dehydrated at 473 K for 2 h. The total surface area was calculated by using the BET equation.

The MTO reaction was performed in a fixed-bed reactor at atmospheric pressure. Typically, 0.4 g sample (sieve fraction, 0.25–0.5 mm) was placed in a stainless steel reactor (internal diameter = 5 mm) and activated under flowing N_2 at 723 K for 1 h. Methanol was injected into the fixed-bed reactor with a flow of 0.5 mL h^{-1} (Weight hour space velocity = 1 h). The reaction products were analyzed utilizing an on-line gas chromatograph equipped with a flame ionization detector and a capillary column Plot Q to separate the C_1-C_8 hydrocarbons. The temperature of the column was maintained at 313 K for 15 min and then increased to 473 K with a rate of 10 K min^{-1}.

The nature of organic compounds formed on the catalysts during the MTO reaction was monitored in situ by FTIR and UV/Vis spectroscopy. The FTIR spectra were recorded in diffuse reflection mode on a Bruker Tensor 27 spectrometer, equipped with a liquid N_2 cooled high sensitivity MCT detector and a DRIFT cell with in situ reaction chamber. The catalyst samples of approximately 25 mg were finely ground and placed in the chamber. Prior to each experiment, the samples were activated in flowing He at 723 K for 1 h and cooled to the desired temperature for a reference spectrum. Then, the same space velocity of methanol as that in the MTO reaction performed in the fixed-bed reactor was fed to the chamber and time-resolved spectra were recorded with a resolution of 4 cm^{-1} and 128 accumulations. The UV/Vis spectra were recorded with an AvaSpec-2048 Fiber Optic spectrometer with an AvaLight-DH-S deuterium light source by Avantes and a glass fiber reflection probe HPSUV1000A by Oxford Electronics. Before the MTO reaction, the glass fiber reflection probe was placed in the fixed-bed reactor on the top of the catalyst with a gap of approximately 1.0 mm. Reference UV/Vis spectra of catalysts were recorded at reaction temperature prior to starting the methanol flow. The in situ UV/Vis spectra were recorded in the range 200–600 nm by using the diffuse reflection mode during the MTO reaction. The amounts of occluded hydrocarbons after the methanol reaction were determined by thermogravimetric analysis on a Rigaku standard type thermogravimetric analyzer. In a typical measurement, 0.1 g of sample was heated in an Al_2O_3 crucible with a constant heating rate of 10 K min^{-1} and under air purging with a flow rate of 30 mL min^{-1}.

The organic compounds formed on the catalysts during the MTO reaction were characterized by ^{1}H and ^{13}C MAS NMR spectroscopy, which was performed on a Bruker Avance III 400WB spectrometer at the resonance frequencies of 400.1 and 100.6 MHz, with $\pi/2$ pulse excitation, high-power decoupling in the case of

^{13}C MAS NMR, repetition times of 10 and 20 s, and with 2.5 and 4 mm MAS NMR probes with sample spinning rates of 25.0 and 12.0 kHz, respectively. ^{13}C MAS NMR spectroscopy of ^{13}C-2-acetone adsorbed on the surface sites of the catalyst samples was used for distinguishing Brønsted and Lewis acid sites. Before the measurements, the samples were dehydrated at 673 K in vacuum (pressure below 10^{-2} Pa) for 12 h. After dehydration, the samples were loaded with 30 mbar ^{13}C-2-acetone for 2 h, and evacuated at room temperature for 5 h to eliminate physisorbed acetone. The Brønsted acid sites were characterized by means of ^{1}H MAS NMR spectroscopy. The samples used for the ^{1}H MAS NMR studies were dehydrated as described above. After dehydration, the samples were sealed and kept in glass tubes until they were loaded into the MAS NMR rotors in a glove box purged with dry nitrogen gas. The determination of the number of accessible Brønsted acid sites was performed upon adsorption of NH_3 at room temperature. After the NH_3 loading, the samples were evacuated at 453 K for 2 h to eliminate physisorbed ammonia. Quantitative ^{1}H MAS NMR measurements were performed by comparing the signal intensities of the samples under study with the intensity of an external intensity standard (dehydrated zeolite H, Na-Y with the cation exchange degree of 35%).

Acknowledgements

This work was supported by the National Basic Research Program of China (2009CB623502), 111 project (B12015), and the Ministry of Education of the People's Republic of China (NCET-11-0251 and IRT0927). Furthermore, M.H. wants to thank for financial support by Fonds der Chemischen Industrie and Deutsche Forschungsgemeinschaft.

Keywords: Brønstead acid sites · heterogeneous catalysis · methanol-to-olefin · mesoporous materials · olefination

[1] M. Stöcker, *Microporous Mesoporous Mater.* **1999**, *29*, 3 – 48.
[2] M. Stöcker, in *Zeolite and Catalysis: Synthesis Reactions and Applications* (Eds: J. Čejka, A. Corma, S. Zones), Wiley-VCH, Weinheim, **2010**, p. 687.
[3] I. M. Dahl, S. Kolboe, *Catal. Lett.* **1993**, *20*, 329 – 336.
[4] I. M. Dahl, S. Kolboe, *J. Catal.* **1994**, *149*, 458 – 464.
[5] I. M. Dahl, S. Kolboe, *J. Catal.* **1996**, *161*, 304 – 309.
[6] B. Arstad, S. Kolboe, *J. Am. Chem. Soc.* **2001**, *123*, 8137 – 8138.
[7] W. G. Song, J. F. Haw, J. B. Nicholas, C. S. Heneghan, *J. Am. Chem. Soc.* **2000**, *122*, 10726 – 10727.
[8] J. F. Haw, W. G. Song, D. M. Marcus, J. B. Nicholas, *Acc. Chem. Res.* **2003**, *36*, 317 – 326.
[9] B. P. C. Hereijgers, F. Bleken, M. H. Nilsen, S. Svelle, K.-P. Lillerud, M. Bjørgen, B. M. Weckhuysen, U. Olsbye, *J. Catal.* **2009**, *264*, 77 – 87.
[10] U. Olsbye, M. Bjørgen, S. Svelle, K. P. Lillerud, S. Kolboe, *Catal. Today* **2005**, *106*, 108 – 111.
[11] S. Wilson, P. Barger, *Microporous Mesoporous Mater.* **1999**, *29*, 117 – 126.
[12] I. M. Dahl, H. Mostad, D. Akporiaye, R. Wendelbo, *Microporous Mesoporous Mater.* **1999**, *29*, 185 – 190.
[13] A. Izadbakhsh, F. Farhadi, F. Khorasheh, S. Sahebdelfar, M. Asadi, Z. F. Yan, *Appl. Catal. A* **2009**, *364*, 48 – 56.
[14] M. J. Van Niekerk, J. C. Q. Fletcher, C. T. O'Connor, *Appl. Catal. A* **1996**, *138*, 135 – 145.
[15] M. A. Djieugoue, A. M. Prakash, L. Kevan, *J. Phys. Chem. B* **2000**, *104*, 6452 – 6461.
[16] Z. Zhu, M. Hartmann, L. Kevan, *Chem. Mater.* **2000**, *12*, 2782 – 2787.
[17] F. D. P. Mees, P. V. D. Voort, P. Cool, L. R. M. Martens, M. J. G. Janssen, A. A. Verberckmoes, G. J. Kennedy, R. B. Hall, K. Wang, E. F. Vansant, *J. Phys. Chem. B* **2003**, *107*, 3161 – 3167.
[18] J. Tan, Z. Liu, X. Bao, X. Liu, X. Han, C. He, R. Zhai, *Microporous Mesoporous Mater.* **2002**, *53*, 97 – 108.
[19] A. Tuel, S. Caldarelli, A. Meden, L. B. McCusker, C. Baerlocher, A. Ristic, N. Rajic, G. Mali, V. Kaucic, *J. Phys. Chem. B* **2000**, *104*, 5697 – 5705.
[20] M. Hunger, *Microporous Mesoporous Mater.* **2005**, *82*, 241 – 255.
[21] L. M. Petkovic, D. M. Ginosar, K. C. Burch, *J. Catal.* **2005**, *234*, 328 – 339.
[22] M. Bjørgen, F. Bonino, B. Arstad, S. Kolboe, K.-P. Lillerud, A. Zecchina, S. Bordiga, *ChemPhysChem* **2005**, *6*, 232 – 235.
[23] J. W. Park, G. Seo, *Appl. Catal. A* **2009**, *356*, 180 – 188.
[24] H. Binder, A. Anikin, B. Kohlstrunk, *J. Phys. Chem. B* **1999**, *103*, 450 – 460.
[25] Y. Jiang, J. Huang, V. R. R. Marthala, Y. S. Ooi, J. Weitkamp, M. Hunger, *Microporous Mesoporous Mater.* **2007**, *105*, 132 – 139.
[26] I. Kirisci, H. Förster, G. Tasi, J. B. Nagy, *Chem. Rev.* **1999**, *99*, 2085 – 2114.
[27] W. Dai, X. Wang, G. Wu, N. Guan, M. Hunger, L. Li, *ACS Catal.* **2011**, *1*, 292 – 299.
[28] J. F. Haw, J. B. Nicholas, T. Xu, L. W. Beck, D. B. Ferguson, *Acc. Chem. Res.* **1996**, *29*, 259 – 267.
[29] S. Li, A. Zheng, Y. Su, H. Zhang, L. Chen, J. Yang, C. Ye, F. Deng, *J. Am. Chem. Soc.* **2007**, *129*, 11161 – 11171.
[30] H. Fang, A. Zheng, Y. Chu, F. Deng, *J. Phys. Chem. C* **2010**, *114*, 12711 – 12718.
[31] Y. Jiang, J. Huang, W. Dai, M. Hunger, *Solid State Nucl. Magn. Reson.* **2011**, *39*, 116 – 141.
[32] M. Hunger, *Catal. Rev. Sci. Eng.* **1997**, *39*, 345 – 393.
[33] H. O. Kalinowski, S. Berger, S. Braun, *^{13}C NMR-Spektroskopie*, Georg Thieme Verlag, Stuttgart, New York, **1984**, p. 136.
[34] G. A. Olah, H. C. Lin, D. A. Forsyth, *J. Am. Chem. Soc.* **1974**, *96*, 6908 – 6911.
[35] G. A. Olah, J. S. Staral, G. Asencio, G. Liang, D. A. Forsyth, G. D. Mateescu, *J. Am. Chem. Soc.* **1978**, *100*, 6299 – 6308.
[36] W. Dai, M. Scheibe, N. Guan, L. Li, M. Hunger, *ChemCatChem* **2011**, *3*, 1130 – 1133.
[37] M. Hesse, H. Meier, B. Zeeh, *Spektroskopische Methoden in der organischen Chemie*, Georg Thieme Verlag, Stuttgart, New York, **1987**, p. 174 – 175.
[38] L. Sommer, A. Krivokapić, S. Svelle, K. P. Lillerud, M. Stöcker, U. Olsbye, *J. Phys. Chem. C* **2011**, *115*, 6521 – 6530.
[39] D. Chen, H. P. Rebo, K. Moljord, A. Holmen, *Ind. Eng. Chem. Res.* **1999**, *38*, 4241 – 4249.
[40] W. Dai, W. Kong, L. Li, G. Wu, N. Guan, N. Li, *ChemCatChem* **2010**, *2*, 1548 – 1551.

Received: December 23, 2011
Revised: February 3, 2012
Published online on July 10, 2012

